

Precision assessment of micro-thruster performance: A comparative study of indium field emission electric propulsion thrust measurement methods with a force-feedback pendulum

Bo-Song Cai(蔡柏松), Yan Shen(沈岩), Yuan Zhong(钟源), Jian-Ping Liu(刘建平), Yu-Qing Wang(王宇清), Zhu Li(李祝), Liang-Cheng Tu(涂良成), and Shan-Qing Yang(杨山清)

Citation: Chin. Phys. B, 2025, 34 (**4**): 045203. DOI: 10.1088/1674-1056/adb9cb
Journal homepage: http://cpb.iphy.ac.cn; http://iopscience.iop.org/cpb

What follows is a list of articles you may be interested in

Upgrade of the magnetic diagnostic system for restart of HT-6M operation

Li-Xing Chen(陈力行), Biao Shen(沈飙), Da-Long Chen(陈大龙), Zheng-Ping Luo(罗正平),Zu-Chao Zhang(张祖超), Ying Chen(陈颖), Yong Wang(王勇), and Jin-Ping Qian(钱金平)

Chin. Phys. B, 2022, 31 (**12**): 125203. DOI: 10.1088/1674-1056/ac7f93

Measurement of molybdenum ion density for L-mode and H-mode plasma discharges in the EAST tokamak

Yongcai Shen(沈永才), Hongming Zhang(张洪明), Bo Lyu(吕波), Yingying Li(李颖颖), Jia Fu(符佳), Fudi Wang(王福地), Qing Zang(臧庆), Baonian Wan(万宝年), Pan Pan(潘盼), Minyou Ye(叶民友)

Chin. Phys. B, 2020, 29 (**6**): 065206. DOI: 10.1088/1674-1056/ab8456

Analysis of extreme ultraviolet spectral profiles of laser-produced Cr plasmas

L Wu(吴磊), M G Su(苏茂根), Q Min(敏琦), S Q Cao(曹世权), S Q He(何思奇), D X Sun(孙对兄), C Z Dong(董晨钟)

Chin. Phys. B, 2019, 28 (**7**): 075201. DOI: 10.1088/1674-1056/28/7/075201

Detailed calibration of the PI-LCX: 1300 high performance single photon counting hard x-ray CCD camera

Wei Hong(洪伟), Xian-Lun Wen(温贤伦), Lai Wei(魏来), Bin Zhu(朱斌), Yu-Chi Wu(吴玉迟), Ke-Gong Dong(董克攻), Chun-Ye Jiao(焦春晔), Bo Wu(伍波), Ying-Ling He(何颖玲), Fa-Qiang Zhang(张发强), Wei-Min Zhou(周维民), Yu-Qiu Gu(谷渝秋)

Chin. Phys. B, 2017, 26 (**2**): 025204. DOI: 10.1088/1674-1056/26/2/025204

Structural and mechanical properties of Al-C-N films deposited at room temperature by plasma focus device

Z A Umar, R Ahmad, R S Rawat, M A Baig, J Siddiqui, T Hussain

Chin. Phys. B, 2016, 25 (**7**): 075201. DOI: 10.1088/1674-1056/25/7/075201

INSTRUMENTATION AND MEASUREMENT

Precision assessment of micro-thruster performance: A comparative study of indium field emission electric propulsion thrust measurement methods with a force-feedback pendulum

Bo-Song Cai(蔡柏松)[1], Yan Shen(沈岩)[1,2], Yuan Zhong(钟源)[3,4,†], Jian-Ping Liu(刘建平)[3,‡], Yu-Qing Wang(王宇清)[3], Zhu Li(李祝)[3], Liang-Cheng Tu(涂良成)[3], and Shan-Qing Yang(杨山清)[3]

[1] *School of Aeronautics and Astronautics, Sun Yat-Sen University (Shenzhen Campus), Shenzhen* 518107, *China*

[2] *Shenzhen Key Laboratory of Intelligent Microsatellite Constellation, Shenzhen* 518107, *China*

[3] *MOE Key Laboratory of TianQin Mission, TianQin Research Center for Gravitational Physics & School of Physics and Astronomy, Frontiers Science Center for TianQin, Gravitational Wave Research Center of CNSA, Sun Yat-Sen University (Zhuhai Campus), Zhuhai* 519082, *China*

[4] *School of Information Engineering, Xinyu University, Xinyu* 338004, *China*

(Received 25 December 2024; revised manuscript received 24 February 2025; accepted manuscript online 25 February 2025)

Accurate thrust assessment is crucial for characterizing the performance of micro-thrusters. This paper presents a comprehensive evaluation of the thrust generated by a needle-type indium field emission electric propulsion (In-FEEP) micro-thruster using three methods based on a pendulum: direct thrust measurement, indirect plume momentum transfer and beam current diagnostics. The experimental setup utilized capacitive displacement sensors for force detection and a voice coil motor as a feedback actuator, achieving a resolution better than 0.1 μN. Key performance factors such as ionization and plume divergence of ejected charged particles were also examined. The study reveals that the high applied voltage induces significant electrostatic interference, becoming the dominant source of error in direct thrust measurements. Beam current diagnostics and indirect plume momentum measurements were conducted simultaneously, showing strong agreement within a deviation of less than 0.2 μN across the operational thrust range. The results from all three methods are consistent within the error margins, verifying the reliability of the indirect measurement approach and the theoretical thrust model based on the electrical parameters of In-FEEP.

Keywords: micro-thruster, field emission, thrust stand, micro-thrust measurement, calibration, pendulum

PACS: 52.25.Tx, 52.75.Di, 79.70.+q, 94.05.–a

DOI: 10.1088/1674-1056/adb9cb **CSTR:** 32038.14.CPB.adb9cb

1. Introduction

Field emission electric propulsion (FEEP), a type of electrostatic micro-thruster based on liquid-metal ion sources (LMISs), exhibits several advantageous characteristics, including a low thrust limit, high thrust resolution, minimal thrust noise, high specific impulse, high efficiency, rapid response time and a compact structure. These attributes position FEEPs as a promising candidate to act as the actuator of drag-free or fine attitude control in space missions.[1–3]

A precise thrust testing procedure conducted on the ground is essential for characterizing and evaluating the performance of FEEP micro-thrusters. This methodology typically involves the simultaneous measurement of current and voltage to validate the thrust model. While this approach is simple and efficient, it is significantly dependent on the underlying model.[4,5] Various factors, including charge-to-mass ratio and plume divergence, may affect the accuracy of the calculations. So as a supplement, current assessments of thruster performance also encompass both direct and indirect thrust measurement utilizing thrust stands.[6] The direct method involves the installation of thrusters onto the measurement system to obtain counter thrust, whereas the indirect method entails placing a receiver plate in the trajectory of the plume jet to measure thrust through momentum transfer,[7] commonly referred to as the plume shooting method.[8]

Direct thrust measurement is regarded as a reliable and precise method for characterizing a thruster's thrust. However, measuring very small thrusts of the order of micro-Newtons presents significant challenges. The pendulum's performance can be adversely affected by mechanical stresses, such as those introduced by power and signal cables connecting the thruster to the test setup. For instance, the cables associated with an indium FEEP (In-FEEP) system, which are responsible for heating, temperature measurement and the application of electrical potential differences, may exert additional varying moments on the pendulum arm. Furthermore, the elevated operating voltage of an In-FEEP often leads to increased electrical interference with the thrust measurement apparatus, resulting

†Corresponding author. E-mail: zhongy257@mail2.sysu.edu.cn

‡Corresponding author. E-mail: liujp39@mail.sysu.edu.cn

© 2025 Chinese Physical Society and IOP Publishing Ltd. All rights, including for text and data mining, AI training, and similar technologies, are reserved.

in larger measurement errors. During testing, the extent of electrostatic interference is influenced by the position of the thruster within the vacuum chamber, suggesting that the volume of the vacuum apparatus should be maximized when possible. For example, when Cesare *et al.* tested the performance of an In-FEEP and Cs-FEEP, they used a cylindrical vacuum chamber with dimensions of $\Phi 1.2\ \mathrm{m} \times 2.5\ \mathrm{m}$.[9] Additionally, Mühlich *et al.* conducted both direct thrust measurements using a torsion pendulum and indirect plume diagnostics for a multi-needle In-FEEP at high thrust levels in a vacuum chamber with dimensions $\Phi 2.2\ \mathrm{m} \times 3\ \mathrm{m}$. The results were in agreement within 5% over a thrust range of 50 μN to 450 μN.[10]

The aforementioned direct thruster testing studies were significantly affected by environmental factors and resulted in increased experimental costs. To mitigate these issues, it is essential for the thrust test device to operate independently of the thruster and its external connections.[5] This configuration allows the thrusters to be directed at a target plate on the pendulum arm for thrust injection, thereby reducing the electrostatic field interference caused by high voltage on the low-potential frame, base, receiver plate and the walls of the vacuum chamber. Additionally, this approach can help minimize the impact of temperature fluctuations on the thrust measurement setup. Therefore, employing the indirect plume momentum measurement method to assess the thrust generated by micro-thrusters is another strategy for performance verification.

All three thrust measurement methods are feasible, but each still has certain problems and limitations for accurate assessment of the performance of FEEP systems.[3,6,10,11] This study conducted a comparative analysis of beam current diagnostics and indirect measurement methods against direct thrust measurements. This involved simultaneous electrical parameter measurements during the indirect plume momentum tests to mitigate inaccuracies arising from the measurement system's conversion processes. Following a series of calibrations, the research considered the electrostatic interference generated by the FEEP during testing. By comparing theoretical and experimental data, the reliability and validity of both the thrust calculation model and the indirect thrust testing methodology were validated.

2. Experimental setup and three measurement methods

2.1. Thrust test platform

Thrust measurements in the micro-Newton range impose stringent requirements on the testing apparatus. The configuration of the thrust stand utilized for indirect thrust testing is depicted in Fig. 1. The testing apparatus primarily comprises an aluminum alloy frame, a crossbeam, springs, counterweights and their respective mounting and adjustment assemblies, as well as electromagnetic voice coils, a high-precision capacitive displacement transducer and electrostatically calibrated plates. The pendulum test system, which employs beryllium bronze springs, is designed to facilitate both direct and indirect thrust testing across a broad frequency spectrum.[12]

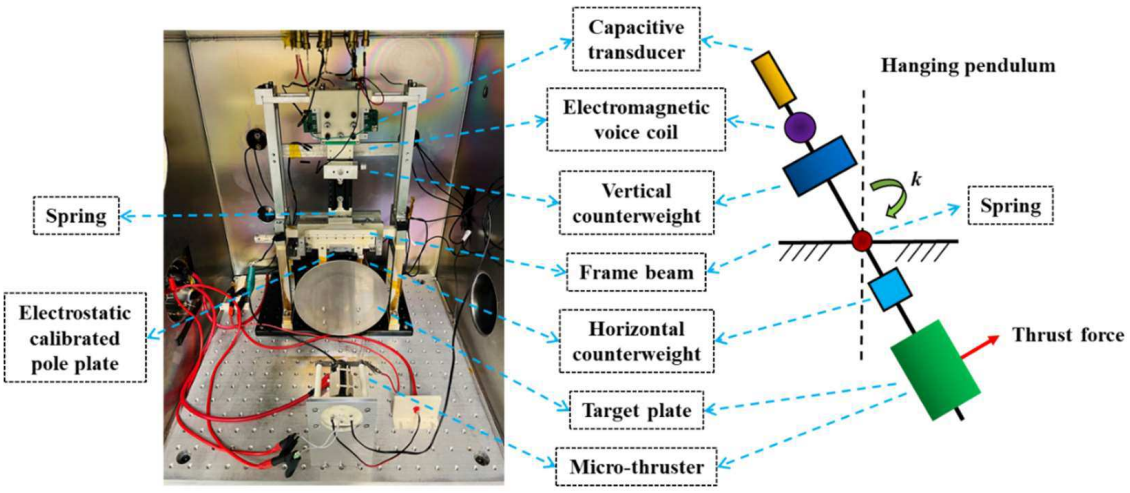


Fig. 1. Experimental apparatus for the thrust test platform.

The commissioning and calibration procedures for the thrust stand encompass the following steps: (i) the capacitive plates are aligned to be parallel; (ii) the dynamic plate is adjusted to ensure it is horizontally centered; (iii) the thrust stand is positioned on the vibration modulation platform and the center of mass of the pendulum arm is vertically adjusted to approximate the swing point of the springs, thereby effectively mitigating noise interference resulting from ground vibrations; (iv) the pendulum is calibrated utilizing electrostatic force, and the background noise of the thrust stand is subsequently assessed.

Ground vibration constitutes a significant factor affecting

the micro-thrust test. Analysis indicates that the coupling of ground vibration to the pendulum is directly proportional to the distance between the center of mass and the suspension point.[12] Therefore, during the debugging phase, efforts are made to align the center of mass with the suspension point of the pendulum as closely as possible in both horizontal and vertical orientations. This alignment effectively mitigates the effect of ground vibration. Additionally, this study implemented a system of suspended pumps and welded bellows to achieve vibration isolation for the vacuum pumps utilized in the laboratory, as shown in Fig. 2.

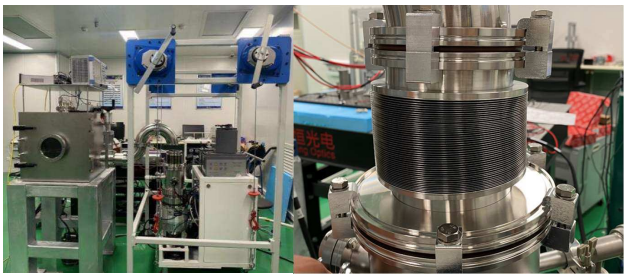


Fig. 2. The experimental setup for the vibration isolation program of suspension and bellow connection for the vacuum pump unit.

The power spectral density of the force noise measurement for the suspended pendulum is presented in Fig. 3. Due to limitations in the precision of manual adjustment, the exact null position of the center of mass of the thrust stand cannot be determined with certainty, introducing a systematic offset uncertainty of ± 0.4 mm in the alignment procedure. Following the adjustment of the center of mass to a position near the pivot point (0.2 ± 0.4 mm), the background noise of the testing system was found to be less than 0.1 μN·Hz$^{-1/2}$ within the frequency range of 0.01 Hz to 3 Hz. This level of noise meets the criteria necessary for the accuracy of micro-thrust testing.

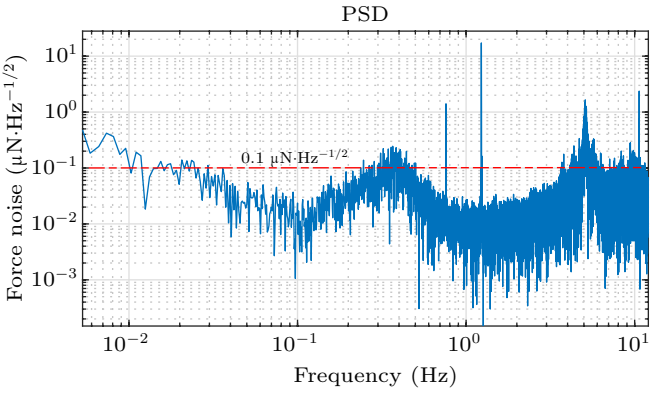


Fig. 3. Power spectral density (PSD) for the background noise of thrust test platform.

2.2. Beam current diagnostics

Thrust serves as a critical metric for evaluating the performance of micro-thrusters. The following analysis pertains to a single cluster of charged particles in motion within an electric field.

The principle of conservation of energy, which encompasses the transformation of potential energy into kinetic energy, can be expressed as follows:

$$Uq = \frac{1}{2}mv^2 - \frac{1}{2}mv_0^2. \tag{1}$$

The momentum theorem is given as follows:

$$F \cdot \Delta t = mv - mv_0. \tag{2}$$

Charge of the particle cluster is determined as follows:

$$q = I \cdot \Delta t, \tag{3}$$

where U is the applied field emission potential difference, m and q are the total mass and total charge of the emitted propellant particle cluster, respectively, v_0 and v are the initial and final velocities of the charged particle cluster in the acceleration process, respectively, and v_0 is more than two orders of magnitude smaller than v, which can be ignored, F is the thrust generated during the particles ejection process, I is the field emission current and Δt is the field emission time.

Assuming that there is no energy loss during the field emission from the micro-thruster and considering the incomplete ionization of the propellant, the theoretical thrust expression for the FEEP can be derived by integrating Eqs. (1)–(3) as follows:

$$\begin{aligned} F &= I \cdot \sqrt{\frac{2mU}{q}} = I \cdot \sqrt{\frac{2U}{\tilde{q}}} = \eta_{\text{ion}} \cdot I \cdot \sqrt{\frac{2m_{\text{ion}}U}{q_{\text{ion}}}} \\ &= \eta_{\text{ion}} \cdot I \cdot \sqrt{\frac{2U}{\tilde{q}_{\text{ion}}}}, \end{aligned} \tag{4}$$

where m_{ion} and q_{ion} are the mass and charge of the individual ions of the emitted propellant ($m_{\text{ion}} = 1.907 \times 10^{-25}$ kg) and the electric charge of In^+ ($q_{\text{ion}} = e = 1.602 \times 10^{-19}$ C), respectively, $\tilde{q} = q/m$ is the charge-to-mass ratio of the emitted propellant particles, $\tilde{q}_{\text{ion}} = q_{\text{ion}}/m_{\text{ion}}$ is the charge-to-mass ratio of the stable-state pure-ion emission mode and η_{ion} is the ionization coefficient. When the field emission current I is small and In is completely ionized, it can be assumed that the emitted charged particles are almost all In^+ (i.e., $\eta_{\text{ion}} \approx 1$).[13]

For externally wetted solid-needle indium LMISs (In-LMISs), this study defines the critical current for stable emission of a FEEP in a pure ionic form as 15 μA, which serves as the experimental upper limit. Theoretically, the critical current falls within the range of 12.7 μA to 15.8 μA, consistent with the Taylor cone stability criterion under the given operating conditions.[14] When the emission current is below this critical threshold, the charge-to-mass ratio of the emitted products remains relatively constant, showing minimal variation with changes in the emission current. It is assumed that at low thrust levels the emission products predominantly consist of singly charged In^+, accounting for approximately 98% of the total

emitted current and thrust contribution.[15] Under these conditions, the emission regime can be characterized as a stable-state pure-ion emission mode, where the charge-to-mass ratio reaches its maximum value of $\tilde{q} = \tilde{q}_{\text{ion}} = 8.4 \times 10^5$ C/kg, and the mass efficiency is considered to be 100%. However, once the emission current surpasses the critical current, a notable decline in mass efficiency is observed. The mass efficiency is quantitatively defined by the following expression:[16–18]

$$\eta = \frac{m_{\text{ion}}}{e} \cdot \frac{\int I \,\mathrm{d}t}{\Delta m} \approx \frac{\tilde{q}}{\tilde{q}_{\text{ion}}} = \left(\frac{I}{I_{\text{c}}}\right)^{\alpha}, \tag{5}$$

where Δm is the total mass loss of FEEP propellant before and after the field emission ($\Delta m \approx m$), $I_{\text{c}} = 0.0005R^2 - 0.1085R + 10.121$ is the critical current, with the units of R and I_{c} as μm and μA, respectively, α is a function of the apex radius of emitting tips R when $I \geq I_{\text{c}}$ and $\alpha = -0.15R \times 10^6 + 0.0698$ ($R < 5.8$ μm). If the emission current is greater than the critical current, the mass efficiency decreases with increase in the field emission current and the apex radius.

The relationship between the ionization coefficient and mass efficiency can be expressed as follows:

$$\eta_{\text{ion}} = \sqrt{\frac{\tilde{q}_{\text{ion}}}{\tilde{q}}} = \frac{1}{\sqrt{\eta}}. \tag{6}$$

The corresponding mass efficiency can be determined based on the parameters I and R, from which η_{ion} can subsequently be derived from η.

In practical applications, a FEEP system exhibits a specific divergence angle in its ejected plume. This divergence angle not only results in a portion of the working substance being ionized directly within the extractor electrode, thereby affecting the performance and longevity of the thruster, but it also contributes to a loss of momentum associated with the thrust vector, which in turn affects the output thrust value. The thrust vector is formed through the superposition of numerous momentum components. The axial projection of charged particle ejection velocity contributes to effective thrust generation. However, plume divergence induces axial momentum loss, with the magnitude of thrust degradation scaling monotonically with increasing divergence angle. Consequently, the actual thrust generated, affected by the divergence of charged particles, is expected to be less than the value theoretically calculated in Eq. (4), necessitating a correction.

For In-FEEP micro-thrusters, considering the divergence of the emission plume, the corrected expression for the actual thrust can be articulated as follows:[19]

$$F_{\text{C}} = \eta_{\text{div}} \cdot F = \eta_{\text{ion}} \cdot \eta_{\text{div}} \cdot I \cdot \sqrt{\frac{2U}{\tilde{q}_{\text{ion}}}}, \tag{7}$$

where η_{div} is the divergence coefficient, which indicates the degree of divergence of the working substance emitted from the emitting tip through the extractor electrode. Therefore η_{div} represents the correction factor for thrust loss due to the plume divergence. By performing an ion beam diagnostic analysis of an In-FEEP, the expression for η_{div} can be given as $(1 - \cos 2\theta_{\text{div}})/(4 - 4\cos\theta_{\text{div}})$,[3,20] where θ_{div} is the plume divergence half-angle of the micro-thruster. The larger the divergence angle is, the smaller the correction factor η_{div} is, which induces a larger axial momentum loss of the beam. The relationship between θ_{div} and I as well as U can be given by an ion beam analysis experiment ($I < 37$ μA, $U < 7$ kV).[21] The larger the field emission voltage and current are, the larger the plume divergence angle is within the range of values of applicable conditions.

Experimental evidence indicates that the thrust loss attributable to plume divergence is typically estimated to be $20\% \pm 10\%$ across the majority of the thrust range,[22] with η_{div} approximating to 0.8.[20] However, under the low-thrust operating conditions investigated in this work (< 5 μN), η_{div} exhibits a rapid increase to values exceeding 0.9. This trend correlates with thrust reduction and is further amplified by decreased U, I and θ_{div}, which collectively lead to a diminished extent of plume divergence. Direct thrust measurements of In-propellant single-emitter In-FEEP-25 and In-FEEP-100 systems, conducted by ONERA France for ARCS,[3] demonstrate excellent agreement with the trend of variation of the correction factor η_{div} obtained in the present study. The primary factors affecting the thrust magnitude of FEEP micro-thrusters include U, I, η_{ion} and η_{div}.

Consequently, by measuring the ion beam current I collected by a target plate and the operating voltage U, and substituting the tip radius R of the needle emitter, the ionization coefficient η_{ion} and plume divergence coefficient η_{div} can be determined. These values are then used to solve for the thrust in the theoretical calculation model Eq. (7).

2.3. Indirect plume momentum measurement

In comparison with the direct test utilizing a hanging pendulum, the indirect plume momentum measurement method offers enhanced assurance that the pendulum's performance remains unaffected. This approach mitigates the additional stiffness that may arise from the connection of cables to the springs. Furthermore, it diminishes the risk of conductive discharge from the internal wiring when a high voltage is applied, thereby safeguarding the power supply from potential overloads within a specified range. Additionally, this method significantly lessens the effect of electrostatic forces generated by the micro-thrusters on the pendulum during high-voltage input. Furthermore, it alleviates the effect of temperature fluctuations on the springs of the thrust stand, which may result from the heating of the working substance (In, purity $\geq 99.999\%$).

Displacement changes the pendulum swing arm due to

the impact of the thruster plume on the target plate, and the impact force generated by the plume can be indirectly measured through the capacitive displacement detection in order to characterize the actual value of the thrust generated by the thruster. The principles and experimental setup for beam current diagnostics, as well as the method for indirect plume momentum measurement, are illustrated in Fig. 4. The measurement apparatus resembles a direct test of a suspended pendulum, with a metal target plate substituting the previous position of the thruster, which is installed and secured at the lower end of the pendulum. The thruster is affixed to a metal frame at a specified distance from the target plate, ensuring that the central axis of the emitted plume aligns with the center of the target plate. Upon the effect of the FEEP plume on the target plate, the kinetic energy of the charged particles within the plume is transformed into internal energy within the target plate. This interaction exerts a force on the surface of the target plate, resulting in movement of the pendulum and generating a moment at the center of the motion of the pendulum arm.

Figure 4(a) is a schematic diagram of the indirect thrust test stand with a hanging pendulum, which illustrates the core components and layout of the experimental setup used to indirectly measure the thrust generated by the In-FEEP microthruster. L_C (moment arm for thrust measurement) represents the distance between the center of the thruster's plume (i.e., the emission of charged particles) and the pivot point of the pendulum. This moment arm is crucial for determining the torque generated by the thrust, which can then be used to calculate the actual thrust force through mechanical principles. L_E (moment arm for electrostatic force calibration) represents the distance moved during the electrostatic force calibration process. Calibration is essential to ensure the accuracy of the thrust measurements. By applying a known high-precision electrostatic force and correlating it with the output voltage of the thrust stand, we determine the system's calibration coefficients. This methodology enables system calibration and error mitigation, thereby ensuring the reliability of thrust measurements generated by the propulsion system.

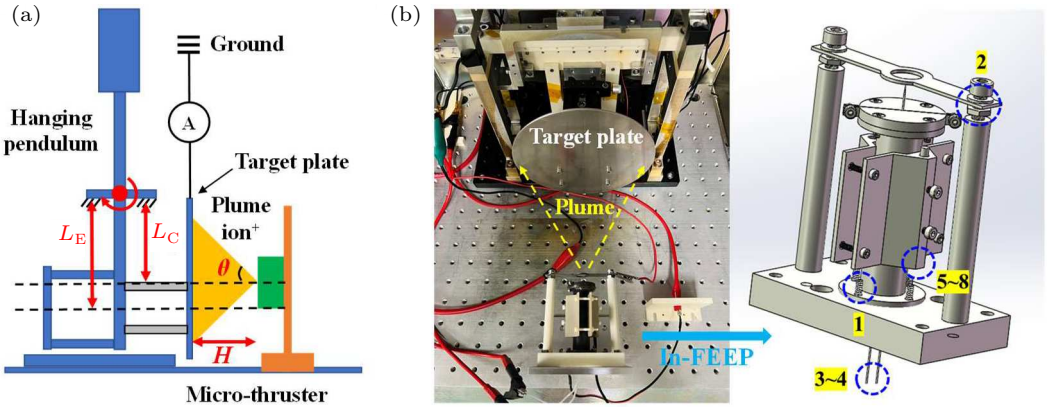


Fig. 4. Principle (a) and device (b) schematic for electrical parameter measurement and the target shooting method in an indirect thrust test of an In-FEEP micro-thruster through a hanging pendulum. Note: in (a) L_C is the moment length between the plume center and the swing point of the thrust stand and L_E is the moment length of the electrostatic force calibration. In panel (b), the wiring configuration of In-FEEP is 1, high-voltage connection for the emitter; 2, ground or negative voltage; 3–4, heating system connections to maintain the molten state of In propellant; 5–8, temperature measurement lines for feedback to regulate the propellant's temperature.

Figure 4(b) shows the device diagram of the electrical connections and wiring configuration of the In-FEEP microthruster. The thruster operates through various electrical inputs that control its operation, including high voltage, ground or negative voltage, heating and temperature measurement. Interface 1 supplies the high voltage required for field emission. In FEEP thrusters, a high electric field is applied to the liquid metal to ionize it and accelerate the ions, generating thrust. The high voltage is a critical component for ionizing the In and initiating the emission process. Interface 2 serves as either the ground connection or provides a negative voltage, depending on the specific electrical configuration of the thruster. It helps create the necessary potential difference between the emitter and the extractor electrode, which is essential for field emission. Interfaces 3–4 are used to heat the indium propellant. In a FEEP thruster, the propellant needs to be in a molten state for efficient ionization and emission. The heating element ensures that the In reaches the required temperature for proper operation. Without sufficient heating, the In might not reach the liquid phase, thus preventing ion emission. Interfaces 5–8 are connected to temperature sensors that monitor the operating temperature of the thruster. Accurate temperature control is vital to ensure that the In remains in the appropriate liquid state and that the thruster operates within safe thermal limits. These measurements also help to maintain the stability and efficiency of the thruster over time.

The recoil of charged particle plumes and sputtering of target metal atoms contribute to the indirectly measured force. Under conditions of perfectly elastic collisions where normal momentum is conserved, the force measured at the target plate is twice the thrust generated by the propulsion system. Conversely, for perfectly inelastic collisions, the mea-

sured force is equal to the actual thrust value. The process by which the target plate receives a plume of charged particles is affected by the superposition of various collision types, including perfectly elastic collisions (both diffuse and specular reflection),[23] perfectly inelastic collisions and inelastic collisions.[24] The diffuse reflection coefficient is $2/3$, the specular reflection coefficient is $1/2$ and the overall restitution coefficient for collisions e ranges from 0 to 1. For partially elastic collisions, the force scales as $F_{\text{measured}} = (1+e)\cdot F_{\text{thrust}}$. The effects of inelastic collisions are contingent upon several factors, including the type of the incident charged particle, the material composition of the target plate surface and the energy of the incident ions.[25]

The complex effects of particle reflection during inelastic collisions, contributing opposite momentum to the normal direction of the target plate, as well as the sputtering of metal atoms and secondary electron emission, are not considered in the thrust measurements.[26–30] Based on these assumptions, the coupling coefficient is approximated as 1. Therefore, the thrust measured by the thrust stand for the micro-thruster is expressed as follows:

$$F_{\text{Indirect}} = F_{\text{T-Thruster}} \cdot \frac{L_{\text{E}}}{L_{\text{C}}} = (F_{\text{T-Indirect}} - F_{\text{E-Indirect}}) \cdot \frac{L_{\text{E}}}{L_{\text{C}}}, \quad (8)$$

where $F_{\text{T-Thruster}}$ is the thrust of the micro-thruster on the target plate, $F_{\text{T-Indirect}}$ is the output thrust of the thrust stand and $F_{\text{E-Indirect}}$ is the electrostatic force on the target plate.

For the indirect plume momentum measurement, a circular aluminum target plate with a radius of $R_{\text{T}} = 80$ mm is employed, positioned at a distance $H = 13$ cm from the In-FEEP micro-thruster. The moment lengths for the plume center and the electrostatic force calibration are designated as $L_{\text{C}} = 83$ mm and $L_{\text{E}} = 117$ mm, respectively. Utilizing the values of R_{T} and H, the maximum divergence angle, $(\theta_{\text{div}})_{\max}$, can be calculated using $(\theta_{\text{div}})_{\max} = \arctan(R_{\text{T}}/H) = 31.61°$. By ensuring that θ_{div} remains less than or equal to $(\theta_{\text{div}})_{\max}$, it is possible to guarantee that the target plate captures the entirety of the plume.

2.4. Direct thrust measurement

The direct measurement of micro-thrust is contingent upon mechanical interaction between the pendulum and FEEP system. Although this method may exhibit less stability than indirect testing, it yields results that are more realistic and reliable. The high-stiffness springs incorporated in the pendulum enhance the system's bandwidth and facilitate electrical connections, thereby mitigating disturbance forces arising from the cables. Figure 5(a) depicts the device system employed for the In-FEEP direct thrust test, which includes the ignition phenomenon. The configuration of the thrust stand springs connected to the thruster is illustrated in Fig. 5(b). This setup comprises six springs linked to the pendulum stand and ground, as well as connections to the input of the electrostatic plate, the low voltage of the extractor electrode, the high voltage of the emitter and the heating device for the working substance (two wires). To prevent breakdown and interference, the high-voltage spring is positioned at a distance of 20 mm or more from the adjacent springs on either side. The thruster is secured using four aluminum support screws, which are strategically placed to minimize contact surfaces and maximize distance from the thrust stand.

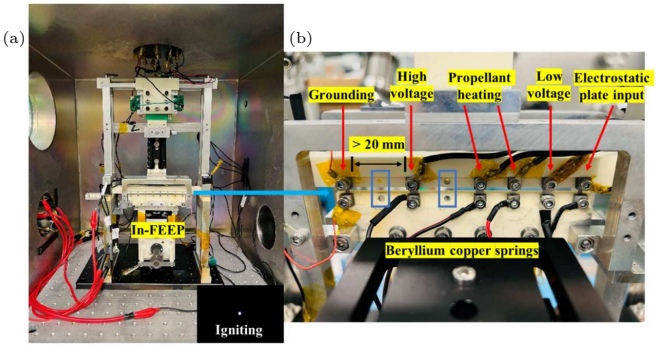


Fig. 5. Assembly diagram of an In-FEEP micro-thruster and thrust stand joint testing system. (a) Installation of thruster to the hanging pendulum and emission plume. (b) Wiring configuration for the six-spring suspension system on the thrust stand.

3. Results and discussion

3.1. Electrostatic force calibration for thrust stand

Calibration serves as a critical assurance of the reliability of the thrust stand outputs. This study employed a non-contact calibration method utilizing a suspended pendulum, which involved the application of a continuously varying potential difference between electrostatic plates to generate diverse electrostatic forces.[31] This approach aims to mitigate mechanical impacts within the system, thereby enhancing the measurement accuracy of thrust stand output parameters (voltage steps as discrete control signals or micro-thrust) and advancing the performance characterization. This method has gained widespread acceptance in the domain of micro-thrust testing and offers a significant advantage over traditional calibration techniques, as the device responsible for generating the electrostatic force does not necessitate mechanical contact with the pendulum apparatus.

The standard electrostatic force F_{E} can be continuously varied as a function of the voltage difference U_{E} applied between the electrostatic plates. The relationship between F_{E} and the output voltage U_{p} of the pendulum can be calculated and fitted through electrostatic force calibration. The capacitance of the calibrated pole plates, which have an area of $S = 5.7 \times 5.7$ cm^2 (relative uncertainty $< 0.06\%$) was measured using an LCR meter (Keysight E4980A) to be $C_0 = 58.32 \pm 0.04$ pF (indirect) and 65.47 ± 0.05 pF (direct). The equidistant electrostatic voltage steps $U_{\text{E}} = [40 - 10 - 40]$ V were provided by a high-precision source measure unit (Keysight B2912A),

with $\Delta U_{\mathrm{E}} = 5$ V (relative uncertainty $< 0.02\%$). The NI PXI-6281 acquisition card, along with a LabVIEW program, was utilized to acquire the steps of U_{p} (Fig. 6).

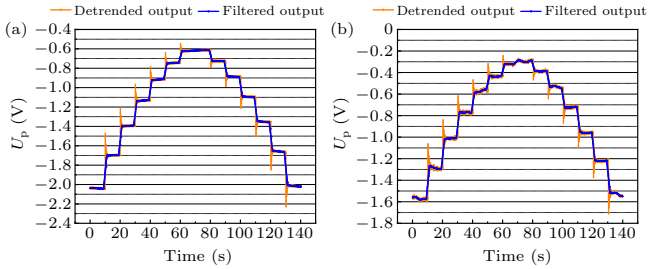


Fig. 6. Output voltage step sampling for electrostatic force calibration of the thrust stand: (a) indirect test; (b) direct test.

The input thrust of the thrust stand is directly proportional to the output voltage $F_{\mathrm{T}} = F_{\mathrm{E}} = k \cdot U_{\mathrm{p}}$. This relationship can be utilized to calculate the calibration coefficient of the testing system as follows:

$$k = \frac{F_{\mathrm{E}}}{U_{\mathrm{p}}} = \frac{C_0^2}{2\varepsilon_0 S} \cdot \frac{U_{\mathrm{E}}^2}{U_{\mathrm{p}}}, \tag{9}$$

where $\varepsilon_0 = 8.854$ pF/m is the permittivity of a vacuum.

In Fig. 7, there is a strong linear correlation between U_{p} and F_{E}. The data can be subjected to linear fitting, allowing for the determination of the calibration coefficients for the test system, which are $k = 62.91 \pm 0.51$ μN/V (indirect) and 90.08 ± 1.26 μN/V (direct).

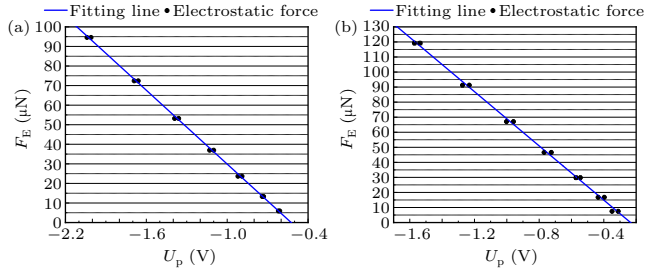


Fig. 7. Calibration curve relating output voltage U_{p} of the hanging pendulum to the standard electrostatic force F_{E}: (a) indirect test; (b) direct test.

3.2. Electrostatic interference in the measurement

The FEEP system was activated and subjected to equidistant voltage increments of $U = [3 - 6 - 3]$ kV, with a voltage step of $\Delta U = 0.5$ kV, under vacuum conditions. The electrostatic forces exerted on the pendulum were measured within the ranges of $F_{\text{E-Indirect}} = (5.87 \pm 0.05)$–$(14.72 \pm 0.12)$ μN and $F_{\text{E-Direct}} = (32.27 \pm 0.45)$–$(129.15 \pm 1.81)$ μN (Fig. 8).

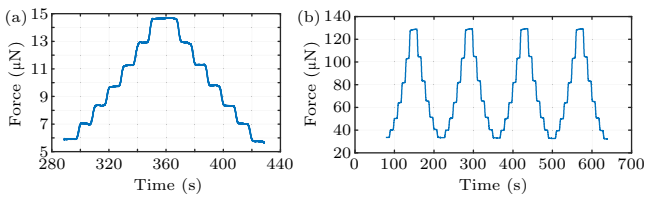


Fig. 8. Electrostatic force response of the thrust stand generated by high-voltage application on an In-FEEP: (a) indirect test; (b) direct test.

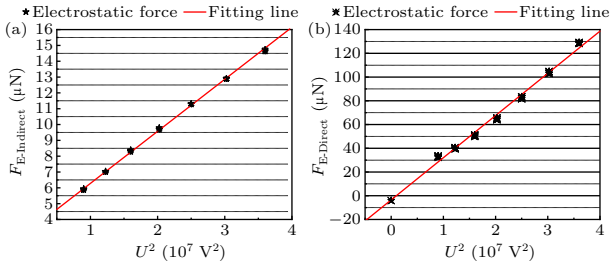


Fig. 9. Relationship between applied voltage to the micro-thruster and electrostatic force on the thrust stand: (a) indirect test; (b) direct test.

The relationship between the applied voltage to the micro-thruster and the resultant electrostatic force was determined through linear regression analysis. The equations derived are as follows: $F_{\text{E-Indirect}} = (3.29 \pm 0.03) \times 10^{-7} \times U^2 + (2.99 \pm 0.05)$ [μN] and $F_{\text{E-Direct}} = (3.55 \pm 0.03) \times 10^{-6} \times U^2 - (3.48 \pm 0.34)$ [μN], with the unit of U as V. These results are illustrated in Fig. 9. A comparative analysis indicates that both the electrostatic interference and the calculation error associated with the direct measurement are an order of magnitude greater than those observed in the indirect measurement. Beyond random errors in measurement data, the dominant sources of uncertainty originate from systematic errors in both electrostatic force calculations for thrust stand calibration and voltage–force correlations, ultimately propagating uncertainty into the electrostatic force characterization model of micro-thrusters.

3.3. Result and analysis

In-FEEP tests were conducted by applying high-voltage steps $U = 4000$–6000 V, with ΔU of 200 V for indirect tests and 500 V for direct tests, all under high-vacuum conditions. During the experimental trials, brief intervals of high-frequency temperature fluctuations exhibited a linear behavior, prompting the implementation of necessary deductions and corrections. Furthermore, the presence of multiple single-frequency signal noises originating from the circuitry adversely impacted the thrust measurement data. To mitigate these effects, the data underwent detrending, followed by the application of a shift-smoothing filter with a window width of 50 specifically designed to eliminate the impact of the two most prominent single-frequency signal perturbations observed at frequencies of 0.7 Hz to 0.8 Hz and 1.2 Hz to 1.3 Hz.

3.3.1. Beam current diagnostics

The theoretical thrust associated with beam current diagnostics is derived from a model based on electrical parameters. This thrust is produced by the rapid injection of field emission products, with its magnitude primarily affected by the field emission current.[32] According to the electrical parameter measurements and calculations from the model, the current range received by the target plate is $I = (13.71 \pm 0.05)$–

(35.05 ± 0.07) μA. In the experimental setup, the measured current is $I_c = 9.89$ μA, leading to a mass efficiency calculated as $\eta = (I/9.89)^{-0.2497}$. This results in a mass efficiency range of $\eta = (92.17\% \pm 0.17\%)$–$(72.91\% \pm 0.05\%)$. Additionally, the ionization coefficient is determined to be $\eta_{\text{ion}} = 1.04$–1.17 (Fig. 10(a)). The mass efficiency decreases gradually with increasing field emission current and voltage, while the ionization coefficient exhibits a corresponding gradual increase, albeit at a slower rate. Consequently, the theoretically calculated thrust is $F = 1.39$–4.91 μN, after which a thrust correction is applied.

The plume divergence half-angle is measured to be $\theta_{\text{div}} = (25.51^\circ \pm 0.10^\circ)$–$(30.01^\circ \pm 0.14^\circ)$, resulting in $\eta_{\text{div}} = (0.95 \pm 0.02)$–$(0.93 \pm 0.07)$ (Fig. 10(b)). The values of θ_{div} are observed to be less than $(\theta_{\text{div}})_{\max}$, at which point the target plate is capable of receiving the entire plume. As the applied voltage and field emission current increase, the plume divergence angle progressively enlarges, leading to a greater loss of axial momentum in the beam and a subsequent reduction in η_{div}. Ultimately, the theoretically corrected thrust can be calculated as $F_C = (1.33 \pm 0.03)$–(4.58 ± 0.33) μN.

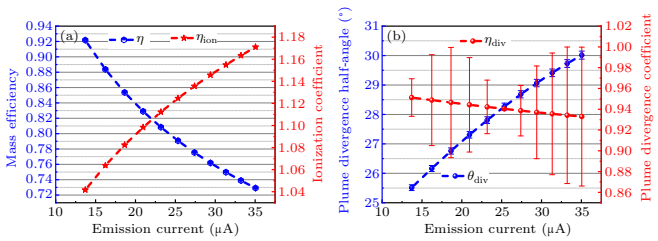


Fig. 10. (a) Variation of mass efficiency and ionization coefficient with field emission current. (b) Variation of plume divergence half-angle and divergence coefficient with field emission current.

3.3.2. Indirect plume momentum measurement

The results obtained from indirect testing indicate that the total thrust output measured by the thrust stand falls within the range of $F_{\text{T-Indirect}} = (9.34 \pm 0.08)$–$(18.14 \pm 0.15)$ μN. Correspondingly, the electrostatic force acting on the thrust stand is observed to be within the range of $F_{\text{E-Indirect}} = (8.25 \pm 0.10)$–$(14.83 \pm 0.16)$ μN (Fig. 11(a)). After accounting for the electrostatic force, the thrust exerted on the target plate by the FEEP system is calculated to be within the range of $F_{\text{T-Thruster}} = (1.07 \pm 0.13)$–$(3.35 \pm 0.22)$ μN. Furthermore, the actual measured thrust, derived from moment conversion, is reported as $F_{\text{Indirect}} = (1.51 \pm 0.18)$–$(4.72 \pm 0.30)$ μN (Fig. 11(b)).

Theoretically, during FEEP operation, the metal target plate functions as an extractor electrode, enhancing the inter-electrode field strength to some extent. This field enhancement promotes propellant ionization and increases the ejection velocity and momentum of charged particles, thereby augmenting thrust generation. However, precise experimental quantification of this effect remains challenging with current methodologies. Based on preliminary numerical simulations, for the operational thrust range of 1–5 μN, the thrust variation ΔF_C remains below 0.01 μN, rendering its impact negligible within the measurement uncertainty.

Figure 11(b) illustrates that as the field emission voltage and current increase, the ratio of the measured thrust F_{Indirect} to the theoretically calculated thrust F decreases. This phenomenon can be attributed to the greater momentum loss of the beam, which is induced by the increased plume divergence angle at elevated voltages, thereby aligning with the theoretical analysis. Furthermore, the trend observed in the FEEP thrust value F_{Indirect}, as measured by the indirect measurement method in this experiment, closely corresponds to the calculated value F_C derived from the theoretical prediction model. As the field emission voltage and current diminish, the thrust generated by the FEEP decreases. However, the rate of change in thrust becomes more gradual, indicating that a higher micro-thrust accuracy can be achieved by the FEEP.

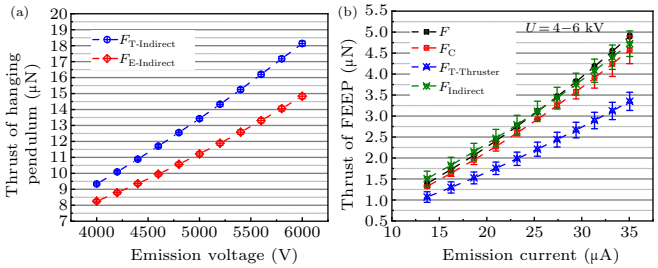


Fig. 11. (a) Variation of output thrust for the thrust stand and electrostatic force produced by the micro-thruster on the target plate with field emission voltage. (b) Variation of theoretical thrust, corrected thrust, thrust on the target plate and measured thrust in indirect testing with a field emission current.

3.3.3. Direct thrust measurement

The results obtained from the direct thrust test indicate that the total thrust range output from the thrust stand is represented as $F_{\text{T-Direct}} = (54.57 \pm 0.77)$–$(129.51 \pm 1.83)$ μN. The electrostatic force generated by the micro-thruster on the thrust stand is quantified as $F_{\text{E-Direct}} = (53.32 \pm 0.59)$–$(124.32 \pm 1.13)$ μN (Fig. 12(a)). By subtracting $F_{\text{T-Direct}}$ from $F_{\text{E-Direct}}$, the thrust of FEEP on the thrust stand, referred to as the actual measured thrust, is calculated to be $F_{\text{Direct}} = (1.25 \pm 0.97)$–$(5.19 \pm 2.15)$ μN. The results of this calculation are depicted in Fig. 12(b).

The theoretical values of FEEP thrust derived from beam current diagnostics are compared with both indirect plume momentum measurements and direct thrust measurements obtained through a hanging pendulum apparatus. This comparison aims to validate the accuracy of the FEEP performance model (Fig. 12(b)). The indirectly measured micro-thrust values exhibit a closer alignment with the theoretically calculated values. Additionally, the red area in Fig. 12(b) represents the

uncertainty introduced by the electrostatic force during the direct testing process, within which both the theoretically predicted and indirectly measured values are situated. Overall, the general trends of FEEP thrust values obtained through the three measurement methods demonstrate a significant degree of compatibility. Under identical experimental conditions, measurements conducted over ten independent trials demonstrate consistent trend alignment with excellent reproducibility, rigorously validating the proposed methodology.

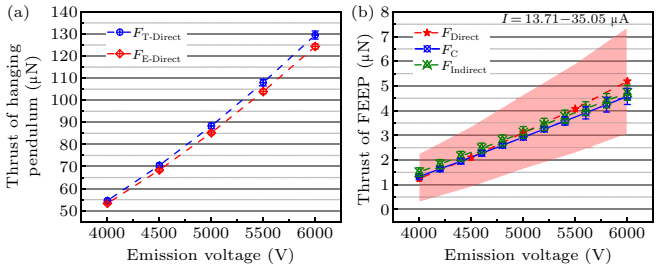


Fig. 12. (a) Output thrust of the thrust stand and electrostatic force generated by a micro-thruster versus applied voltage in a direct thrust test. (b) Comparison of modified thrust calculated by F_{C}, F_{Indirect} and F_{Direct} with the field emission voltage.

The charged particles of the propellant rebound from the surface of the target plate with a specific kinetic energy upon collision, resulting in an impulse transferred to the thrust stand that exceeds the actual impulse generated by the thruster. Therefore, the thrust value recorded by the thrust stand is elevated during this process, and the extent of this overestimation is contingent upon the interaction between the particles and the target plate. A comparative analysis of the indirect measurements with beam current diagnostics revealed that the indirect thrust measurements for the micro-thrust consistently exceed the theoretically calculated thrust across all tested voltage levels and corresponding thrust ranges [4–6 kV, (1.33 ± 0.03)–(4.72 ± 0.30) μN]. The observed discrepancy, which is within 0.18 μN, indicates that the results of the indirect measurements are largely consistent with the theoretical model. Furthermore, as the field emission voltage and current progressively increase, the ratio of F_{C} to F_{Indirect} also increases, as does the ratio of F_{Direct} to F_{Indirect}. The observed phenomena may be attributed to the increase in both U and I, which enhances the impact force of the plume. This, in turn, leads to a greater degree of diffuse reflection of charged particles on the surface of the target plate, indicating an increase in the inelastic collision effect.

4. Conclusion and perspectives

This paper presented a field emission performance evaluation of an In-FEEP micro-thruster using a thrust stand. Multiple methods were employed to characterize the thrust performance, including the electrical parameter prediction model, beam current diagnostics, indirect plume momentum measurement and direct thrust measurement. The study analyzed the factors affecting the accuracy of these tests. Notably, the high voltage applied during the experiments generated substantial electrostatic interference, which proved to be the most significant source of error in direct thrust measurements. The modified theoretical thrust values, accounting for electrostatic forces, ranged from 1.33 ± 0.03 μN to 4.58 ± 0.33 μN, with indirect measurement values between 1.51 ± 0.18 μN and 4.72 ± 0.30 μN, and direct measurement values from 1.25 ± 0.97 μN to 5.19 ± 2.15 μN. Comparison of the three methods demonstrated a high degree of consistency, particularly between the indirect plume momentum measurements and beam current diagnostics, both of which fell within the error margins of the direct thrust measurements and aligned with the average direct measurement results. This experimental verification affirms the reliability and accuracy of the thrust calculation model based on electrical parameters, confirming that the actual thrust of a FEEP can be reliably determined by measuring the field emission current and voltage. However, electrostatic interference had a significant impact on the results, particularly in direct measurements. To enhance the accuracy of future experiments, it is recommended that improvements be made to the structure of the hanging pendulum by incorporating electrostatic shielding to mitigate this interference.

Acknowledgments

Project supported by the National Key Research and Development Program of China (Grant No. 2020YFC2201001), the Guangdong Major Project of Basic and Applied Basic Research (Grant No. 2019B030302001), the National Natural Science Foundation of China (Grant Nos. 12105373, 12105374, and 11927812), and the Science and Technology Research Project of Jiangxi Provincial Department of Education (Grant No. GJJ2402105).

References

[1] Liu H, Niu X, Zeng M, Wang S S, Cui K and Yu D R 2022 *Acta Astronaut.* **193** 496
[2] Gong Y G, Luo J and Wang B 2021 *Nat. Astron.* **5** 881
[3] Genovese A, Steiger W and Tajmar M 2001 37*th Joint Propulsion Conference and Exhibit* (Reston, Virigina: American Institute of Aeronautics and Astronautics) p. 3788
[4] Scharlemann C, Genovese A, Schnitzer R, Buldrini N, Sattler P, Tajmar M, Killinger R and Früholz H 2009 31*st International Electric Propulsion Conference*
[5] Zhang Z, Zhang Z, Xu S T, Ling W Y L, Ren J X and Tang H B 2021 *Aerosp. Sci. Technol.* **110** 106480
[6] Marhold K and Tajmar M 2005 41*st AIAA/ASME/SAE/ASEE Joint Propulsion Conference & Exhibit* (Reston, Virigina: American Institute of Aeronautics and Astronautics) p. 4387
[7] Gessini P, Gabriel S B and Fearn D G 2005 *IEPC Pap.* 05
[8] Courtney D G, Dandavino S and Shea H 2016 *J. Propuls. Power* **32** 392

[9] Cesare S, Musso F, D'Angelo F, Castorina G, Bisi M, Cordiale P, Canuto E, Nicolini D, Balaguer E and Frigot P 2009 31*st International Electric Propulsion Conference* 182

[10] Mühlich N S, Gerger J, Seifert B and Aumayr F 2022 *Acta Astronaut.* **197** 107

[11] Ziemer J K 2001 27*th International Electric Propulsion Conference* 10

[12] Zou S, Cheng Z W T, Zhang X, Wang G F, Liu H F, Yang Z B, Zhong Y, Liu J P, Tu L C, Yang S Q and Li Z 2023 *Phys. Rev. Appl.* **19** 024040

[13] Tajmar M, Genovese A and Steiger W 2004 *J. Propuls. Power* **20** 211

[14] Mair G L R 1996 *J. Phys. D: Appl. Phys.* **29** 2186

[15] Fehringer M, Ruedenauer F and Steiger W 1998 *American Institute of Physics* **456** 207

[16] Tajmar M 2005 *Appl. Phys. A* **81** 1447

[17] Tajmar M and Genovese A 2003 *Appl. Phys. A Mater. Sci. Process.* **76** 1003

[18] Buldrini N, Bettiol L, Seifert B, Plesescu F, Amo J G del and Massotti L 2023 74*th International Astronautical Congress* (Austria)

[19] Kramer A, Bangert P and Schilling K 2020 *Aerospace* **7** 98

[20] Tajmar M, Steiger W and Genovese A 2001 37*th Joint Propulsion Conference and Exhibit* (Reston, Virigina: American Institute of Aeronautics and Astronautics) p. 3790

[21] Mühlich N S, Aumayr F and Leiter H J 2022 *Acta Astronautica* **197** 107

[22] Genovese A, Tajmar M, Buldrini N and Steiger W 2004 *J. Propuls. Power* **20** 219

[23] Grubišić A N and Gabriel S B 2010 *Meas. Sci. Technol.* **21** 105101

[24] Chakraborty S, Courtney D G and Shea H 2015 *Rev. Sci. Instrum.* **86** 115109

[25] Zhang Z, Wang Y, Zhang G, Qi J, Liu J, Tang H and Cao J 2022 *Vacuum* **204** 111384

[26] Weng H Y, Cai G B, Liu L H, Zheng H R, Zhang M X, Zhang B Y and He B J 2021 *Meas. Sci. Technol.* **32** 085301

[27] Wang B, Yang W, Tang H, Li Z, Kitaeva A, Chen Z, Cao J, Herdrich G and Zhang K 2018 *Meas. Sci. Technol.* **29** 075302

[28] Weng H Y, Cai G B, Liu L H, Zheng H R, Shang S F and He B J 2018 *AIP Adv.* **8** 085027

[29] Chakraborty S 2015 *EPFL* Vol. 6645

[30] Williams J D, Johnson M L and Williams D D 2004 40*th AIAA/ASME/SAE/ASEE Joint Propulsion Conference and Exhibit* (Reston, Virigina: American Institute of Aeronautics and Astronautics)

[31] Yan A H, Appel B C and Gedrimas J G 2009 47*th AIAA Aerospace Sciences Meeting including The New Horizons Forum and Aerospace Exposition* (Reston, Virigina: American Institute of Aeronautics and Astronautics) p. 212

[32] Zhong Y, Liu J P, Li Z, Wang Y Q, Li W, Zhang H Y, Zou S, Cai B S, Gong Y W, Tu L C and Yang S Q 2024 *Measurement* **224** 113809